

Direct photon production at HERA, the Tevatron and the LHC

R. E. Blair^a, S. Chekanov^a, G. Heinrich^b, A. Lipatov^c and N. Zotov^c

^a HEP Division, Argonne National Laboratory, 9700 S. Cass Avenue, Argonne, IL 60439, USA

^b Institute for Particle Physics Phenomenology, Department of Physics,
University of Durham, Durham, DH1 3LE, UK

^c SINP, Moscow State University, 119991 Moscow, Russia

Abstract

We review several most recent prompt-photon measurements at HERA and the Tevatron and discuss their implication for future measurements at the LHC. A comparison to Monte Carlo models, as well as to NLO QCD predictions based on the standard DGLAP and the k_T -factorization approaches is discussed. Effects from renormalization and factorization scale uncertainties, as well as uncertainties on the gluon density distribution inside a proton are discussed.

1 Introduction

Events with an isolated photon are an important tool to study hard interaction processes since such photons emerge without the hadronization phase. In particular, final states of ep and pp collisions with a prompt photon together with a jet are more directly sensitive to the underlying QCD process than inclusive prompt photon measurements.

The results on prompt-photon production provided by HERA are important for the interpretation of the LHC data. Unlike pp collisions, ep collisions involve a point-like incoming lepton, which leads to some simplification in the description of the prompt-photon production in ep compared to pp . At HERA, the quark content of the proton is probed through the elastic scattering of a photon by a quark, $\gamma q \rightarrow \gamma q$ (see Fig. 1). Such QED events are significantly simpler than lowest-order Compton-like $qg \rightarrow q\gamma$ events which are dominant in pp collisions (see Fig. 2, left figure). The latter process has direct sensitivity to the strong coupling constant and requires much better understanding of the gluon structure function inside both incoming protons than for the lowest-order diagram in ep collisions.

Despite the difference between ep and pp collisions concerning certain lowest-order diagrams, a large class of partonic contributions are similar between ep and pp collisions, due to the hadronic nature of the resolved photon. In particular, a contribution to prompt-photon events from the $gq \rightarrow q\gamma$ process in photoproduction, in which the photon displays its hadronic structure [1–4], leads to significant sensitivity to the gluon structure function as is the case in pp collisions (see Fig. 2, the two figures on the right). Therefore,

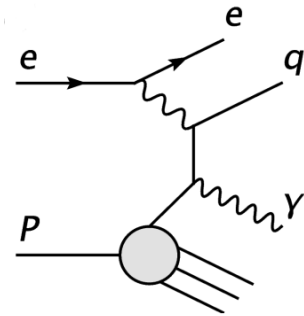


Fig. 1: Lowest-order diagram (Compton scattering) for γ +jet events in ep collisions

analysis of HERA data can make a bridge between a better understood ep case and the less understood pp case, since apart from the convolution with different structure functions, photoproduction diagrams ep collisions involving a resolved photon are essentially the same as diagrams in pp collisions.

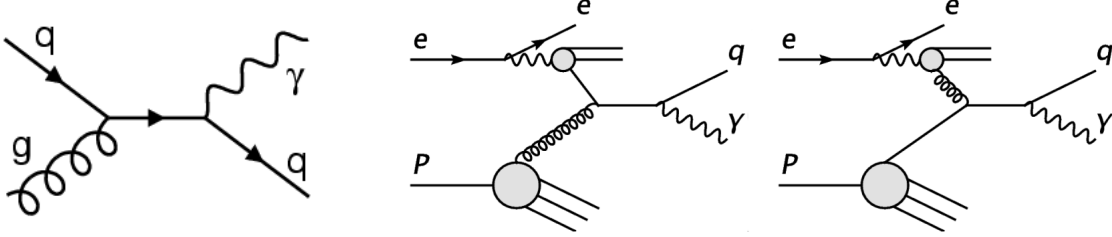


Fig. 2: The dominant diagram for prompt-photon events in pp collisions (left figure) compared to two resolved photon diagrams in ep photoproduction (see Section 2 for more details).

Prompt-photon events in ep collisions can constrain both quark and gluon parton densities (PDFs). In addition, differences between collinear factorization and k_T factorization in the description of the underlying hard subprocesses can be studied in detail. This is important not only for a better understanding of QCD dynamics, but also has direct implications for searches of exotic physics at the LHC, in which prompt-photon production is the main background. A number of QCD predictions [2–6] can be confronted with the data and some of them will be described in more detail below.

2 Photoproduction of prompt photons at NLO

In the photoproduction ep scattering processes, the electron is scattered at small angles, emitting a quasi-real photon which scatters with the proton. The spectrum of these photons can be described by the Weizsäcker-Williams approximation [7]. The photons will take part in the hard interaction either directly, or through their “partonic” content, in which case a parton stemming from the *resolved* photon participates in the hard subprocess. Similarly, a photon in the final state can either originate directly from the hard interaction or from the fragmentation of a parton. Therefore, one can distinguish four categories of subprocesses: 1) direct direct, 2) direct fragmentation, 3) resolved direct and 4) resolved fragmentation. Examples of leading order diagrams of each class are shown in Fig. 3. Beyond leading order, this distinction becomes ambiguous. For example, the NLO corrections to the direct part involve final state collinear quark-photon pairs which lead to divergences which are absorbed into the fragmentation function, such that only the sum of these contributions has a physical meaning. The complete NLO corrections to all four parts have been calculated in [4] for inclusive prompt photons and in [8] for photon plus jet final states. A public program EPHOX, written as a partonic event generator, is available from [9]. The NLO corrections to the direct-direct part also have been calculated in [3, 10] for the inclusive and photon plus jet final state.

The γ - p scattering processes are of special interest since they are sensitive to both the partonic structure of the photon as well as of the proton. They offer the possibility to constrain the (presently poorly known) gluon distributions in the photon, since in a certain kinematic region the subprocess $qg \rightarrow \gamma q$, where the gluon is stemming from a resolved photon, dominates [5].

Working within the framework of collinear factorization, i.e. assuming that the transverse momenta of the partons within the proton can be neglected and other non-perturbative effects can be factorized from the hard interaction at high momentum transfers, the cross section for $ep \rightarrow \gamma X$ can symbolically be written as a convolution of the parton densities for the incident particles (respectively

fragmentation function for an outgoing parton fragmenting into a photon) with the partonic cross section $\hat{\sigma}$:

$$d\sigma^{ep \rightarrow \gamma X}(P_p, P_e, P_\gamma) = \sum_{a,b,c} \int dx_e \int dx_p \int dz F_{a/e}(x_e, M) F_{b/p}(x_p, M_p) D_{\gamma/c}(z, M_F) d\hat{\sigma}^{ab \rightarrow cX}(x_p P_p, x_e P_e, P_\gamma/z, \mu, M, M_p, M_F) , \quad (1)$$

where M, M_p are the initial state factorization scales, M_F the final state factorization scale, μ the renormalization scale and a, b, c run over parton types. In the NLO calculations shown in Fig. 4, all these scales are set equal to p_T^γ and varied simultaneously. The functions $F_{b/p}(x_p, M_p)$ are the parton distribution functions in the proton, obeying DGLAP evolution. Note that including initial state radiation at NLO in the partonic calculation means that the partons taking part in the hard interaction can pick up a nonzero transverse momentum. In certain cases, this additional “ k_T -kick” seems to be sufficient to describe the data well. For example, a study of the effective transverse momentum $\langle k_T \rangle$ of partons in the proton has been made by ZEUS [11]. Comparing the shapes of normalized distributions for $\langle k_T \rangle$ -sensitive observables to an NLO calculation, it was found that the data agree well with NLO QCD without extra intrinsic $\langle k_T \rangle$ [8].

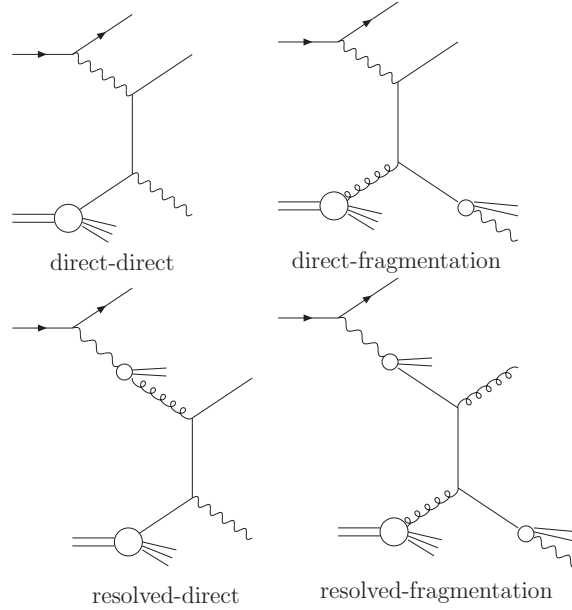


Fig. 3: Examples of contributing subprocesses at leading order to each of the four categories in ep collisions.

The “resolved” contributions are characterized by a resolved photon in the initial state where a parton stemming from the photon instead of the photon itself participates in the hard subprocess. In these cases, $F_{a/e}(x_e, M)$ is given by a convolution of the Weizsäcker-Williams spectrum $f_\gamma^e(y)$ with the parton distributions in the photon:

$$F_{a/e}(x_e, M) = \int_0^1 dy dx_\gamma f_\gamma^e(y) F_{a/\gamma}(x_\gamma, M) \delta(x_\gamma y - x_e) . \quad (2)$$

The cases with “direct” attributed to the initial state photon correspond to $a = \gamma$, so $F_{a/\gamma} = \delta(1-x_\gamma)$ and $F_{a/e}$ in eq. (2) collapses to the Weizsäcker-Williams spectrum. The cases “direct-direct” and “resolved-direct” correspond to $c = \gamma$, so $D_{\gamma/c}(z, M_F) = \delta_{c\gamma}\delta(1-z)$ in (1), i.e. the prompt photon is produced directly in the hard subprocess and not from the fragmentation of a hard parton.

If additional jets are measured, eq. (1) also contains a jet function, which defines the clustering of the final state partons other than the photon into jets. Prompt photon production in association with a jet offers more possibilities to probe the underlying parton dynamics. It allows for the definition of observables that provide information about the longitudinal momentum fractions x^γ, x^p carried by the particles taking part in the hard interaction. The partonic x^γ, x^p are not observable, but one can define the observables

$$\begin{aligned} x_{obs}^\gamma &= \frac{p_T^\gamma e^{-\eta^\gamma} + p_T^{\text{jet}} e^{-\eta^{\text{jet}}}}{2E^\gamma}, \\ x_{obs}^p &= \frac{p_T^\gamma e^{\eta^\gamma} + p_T^{\text{jet}} e^{\eta^{\text{jet}}}}{2E^p}, \end{aligned} \quad (3)$$

which, for direct photons in the final state, coincide with the partonic x^γ, x^p at leading order. Unique to photoproduction processes is the possibility to “switch on/off” the resolved photon by suppressing/enhancing large x^γ . As $x^\gamma = 1$ corresponds to direct photons in the initial state, one can obtain resolved photon enriched data samples by placing a cut $x_{obs}^\gamma \leq 0.9$. Another possibility to enhance or suppress the resolved photon component is to place cuts on p_T and rapidity. From eq. (3) one can easily see that x_{obs}^γ is small at low $p_T^{\gamma, \text{jet}}$ values and large rapidities. Small x^γ -enriched data samples could be used to further constrain the parton distributions in the real photon, in particular the gluon distribution, as investigated e.g. in [5]. Similarly, one can suppress the contribution from the resolved photon to probe the proton at small x^p by direct γ - p interactions [5].

In order to single out the prompt photon events from the background of secondary photons produced by the decays of light mesons, isolation cuts have to be imposed on the photon signals in the experiment. A widely used isolation criterion is the following: A photon is isolated if, inside a cone centered around the photon direction in the rapidity and azimuthal angle plane, the amount of hadronic transverse energy E_T^{had} deposited is smaller than some value $E_{T, \text{max}}$:

$$\text{for } \frac{(\eta - \eta_\gamma)^2}{E_T^{\text{had}}} + \frac{(\phi - \phi_\gamma)^2}{E_{T, \text{max}}} \leq R, \quad (4)$$

HERA experiments mostly used $E_{T, \text{max}} = \epsilon p_T^\gamma$ with $\epsilon = 0.1$ and $R = 1$. Isolation not only reduces the background from secondary photons, but also substantially reduces the contribution from the fragmentation of hard partons into high- p_T photons. When comparing the result of partonic calculation to data, photon isolation is a delicate issue. For example, a part of the hadronic energy measured in the cone may come from the underlying event; therefore even the direct contribution can be cut by the isolation condition if the latter is too stringent.

3 k_T -factorization approach

A complementary description is offered by the k_T -factorization approach [12], which relies on parton distribution functions where the k_T -dependence has not been integrated out.

In the framework of k_T -factorization approach the treatment of k_T -enhancement in the inclusive prompt photon suggests a possible modification of the above simple k_T smearing picture. In this approach the transverse momentum of incoming partons is generated in the course of non-collinear parton

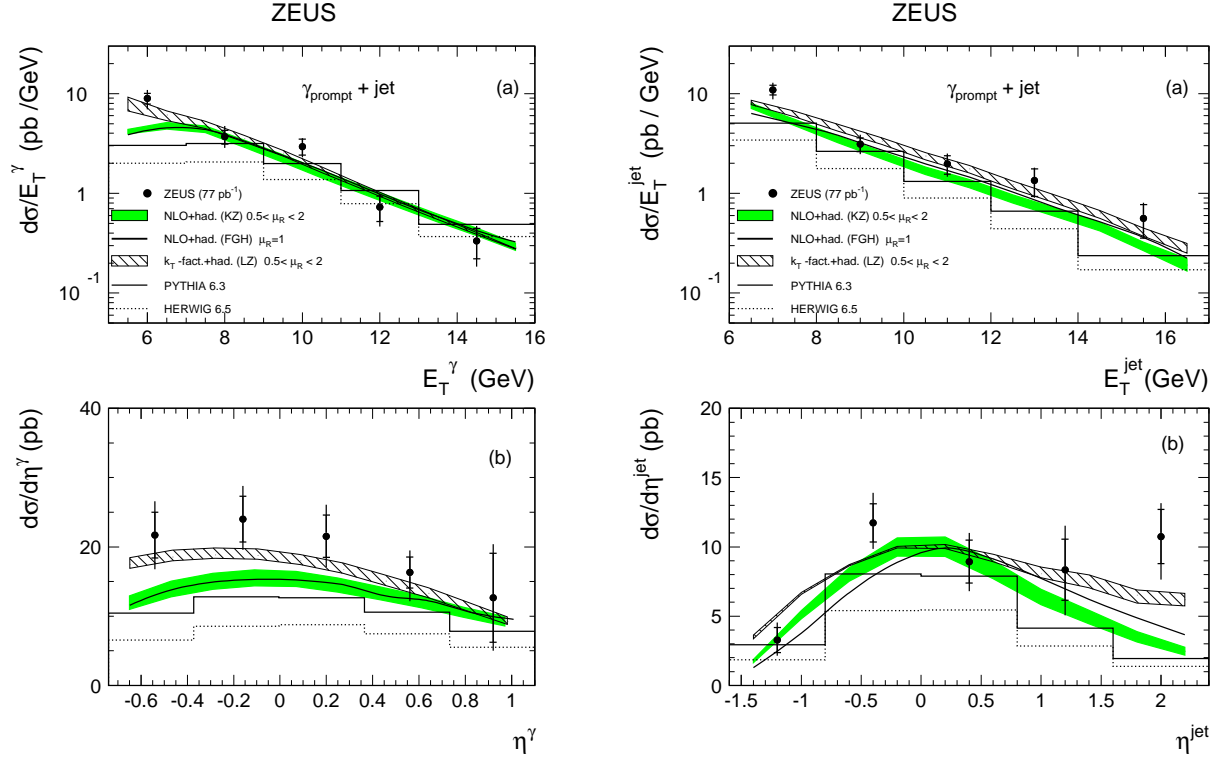


Fig. 4: The differential γ +jet cross sections as functions of E_T and η of the prompt photon and the jet. The data are compared to QCD calculations and Monte Carlo models as described in the text. The shaded bands correspond to a typical scale uncertainty which was obtained by changing the renormalization and factorization scales simultaneously by a factor of 0.5 and 2 respectively.

evolution under control of relevant evolution equations. In the papers [6, 13] the Kimber-Martin-Ryskin (KMR) formalism [14] was applied to study the role of the perturbative components of partonic k_T in describing of the observed E_T spectrum at HERA and Tevatron. The proper off-shell expressions for the matrix elements of the partonic subprocesses and the KMR-constructed unintegrated parton densities obtained independently were used in [13] to analyze the Tevatron data.

4 Comparison with HERA results

Recently published [15] ZEUS differential cross sections as functions of E_T and η for the prompt-photon candidates and for the accompanying jets have revealed some difference with both Monte Carlo predictions and the next-to-leading order (NLO) calculations based on the collinear factorization and the DGLAP formalism [3, 4], as shown in Fig. 4. The data are compared to QCD calculations performed by Krawczyk and Zembrzusi (KZ) [3], by Fontannaz, Guillet and Heinrich (FGH) [4], by A. Lipatov and N. Zotov (LZ) [6] and and PYTHIA 6.4 [16] and HERWIG 6.5 [17] Monte Carlo models. The MC differential cross sections do not rise as steeply at low E_T^γ as do the data. It should be pointed out that no intrinsic transverse momentum of the initial-state partons in the proton was assumed for these calculations. The QCD calculation [6] based on the k_T -factorization [12] and the Kimber-Martin-Ryskin (KMR) prescription [14] for unintegrated quark and gluon densities, gives the best description of the E_T

and η cross sections.

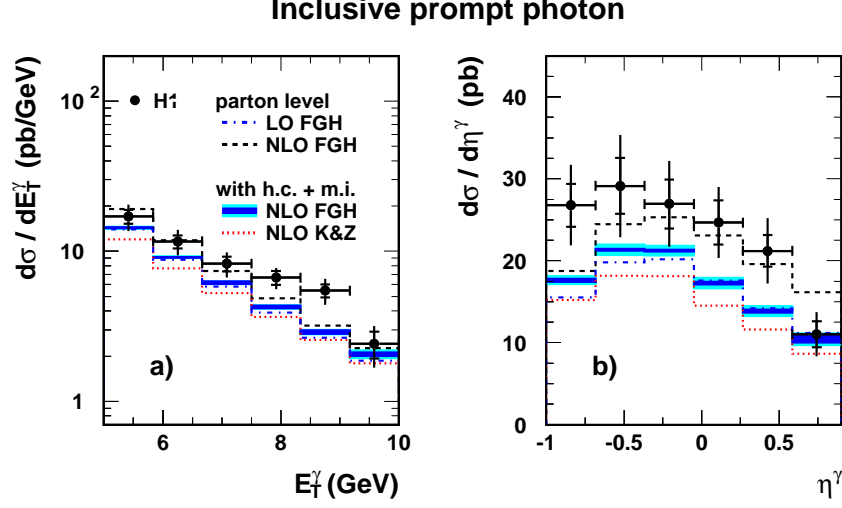


Fig. 5: The differential cross section $d\sigma/dE_T$ and $d\sigma/d\eta^\gamma$ as functions of E_T^γ and η^γ of the inclusive prompt photon photo-production calculated at $-0.7 < \eta^\gamma < 0.9$ and $0.2 < y < 0.9$. The data are compared to two different NLO calculations.

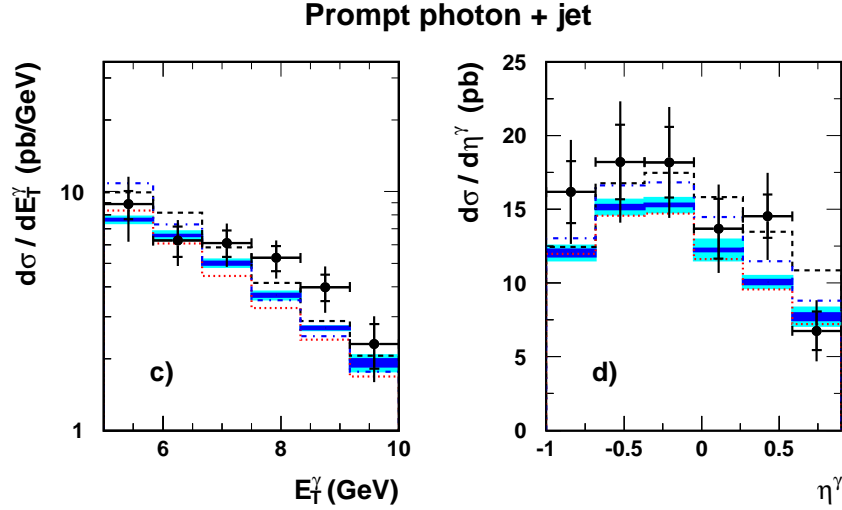


Fig. 6: Same as in Fig. 5, but for γ +jet events with the additional jet cuts: $-1 < \eta^{\text{jet}} < 2.3$ and $E_T^{\text{jet}} > 4.5$ GeV.

In the photon-rapidity distribution of Fig. 4, the data lying above the NLO theory prediction at low values of η^γ could be explained by the fact that in this region, x_{obs}^p is small, as can be seen from Eq. (3), and therefore k_T -effects may be important. On the other hand, this is not corroborated by the jet rapidity distribution, which has a problem at high η^{jet} , corresponding to small x_{obs}^γ . Indeed, a direct measurement [15] of x_{obs}^γ shows that the differences with NLO are mainly at low values of the x_{obs}^γ distribution. In this region, resolved photon events dominate, which may indicate that resolved photon remnants could have lead to an increase in the number of jets which have passed the experimental cuts, while these events are not accounted for in the partonic calculation.

The inclusive prompt photon data [18, 19] lie above the NLO theory prediction in the whole rapidity range, except for the bin of largest rapidity, where the agreement is good after hadronization

corrections, see Fig. 5.

Interestingly, ZEUS investigated what happens if the minimum transverse energy of the prompt photon is increased to 7 GeV, and found that in this case, the NLO calculations are in good agreement [15], which suggests that non-perturbative effects may produce the discrepancy. See [20] and references therein for more details.

The H1 experimental data in photoproduction [18] are shown in Figs. 5 and 6. Both inclusive and γ +jet cross sections were compared to the FGH NLO calculations after hadronization corrections. The H1 data [18] referred to the kinematic region defined by $5 < E_T^\gamma < 10$ GeV, $-1 < \eta^\gamma < 0.9$ and $0.2 < y < 0.7$, which is rather similar to the ZEUS measurement shown in Fig. 4. Similar to the ZEUS case, MC predictions were found to underestimate the H1 cross sections, while NLO QCD gives a much better description. After taking into account hadronization and multiple interaction effects, NLO calculations predict somewhat smaller cross sections compared the measurements [18].

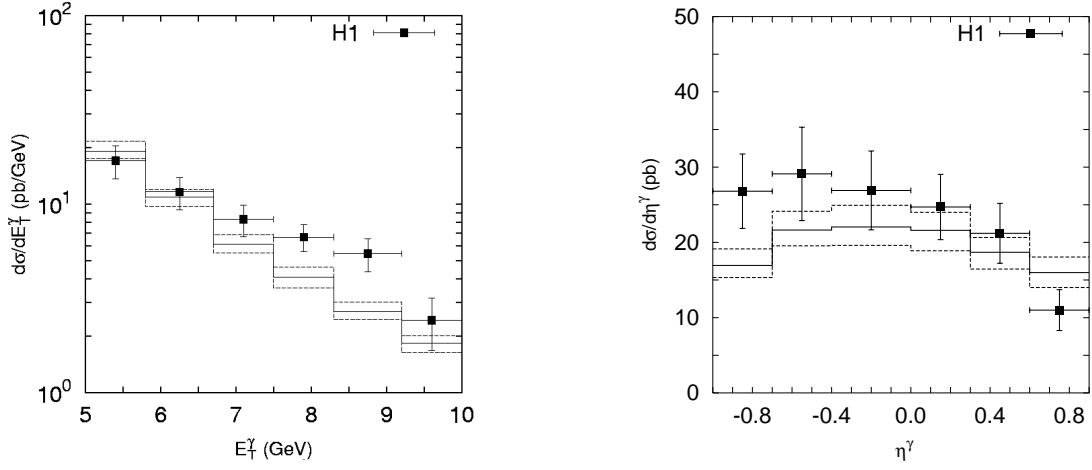


Fig. 7: The differential cross section $d\sigma/dE_T$ and $d\sigma/d\eta^\gamma$ as functions of E_T^γ and η^γ of the inclusive prompt photon photoproduction calculated at $-0.7 < \eta^\gamma < 0.9$ and $0.2 < y < 0.9$. The data are compared to the k_T -factorization calculations. The bands correspond to a typical renormalization scale uncertainty which was obtained by changing μ_R by a factor of 0.5 and 2.

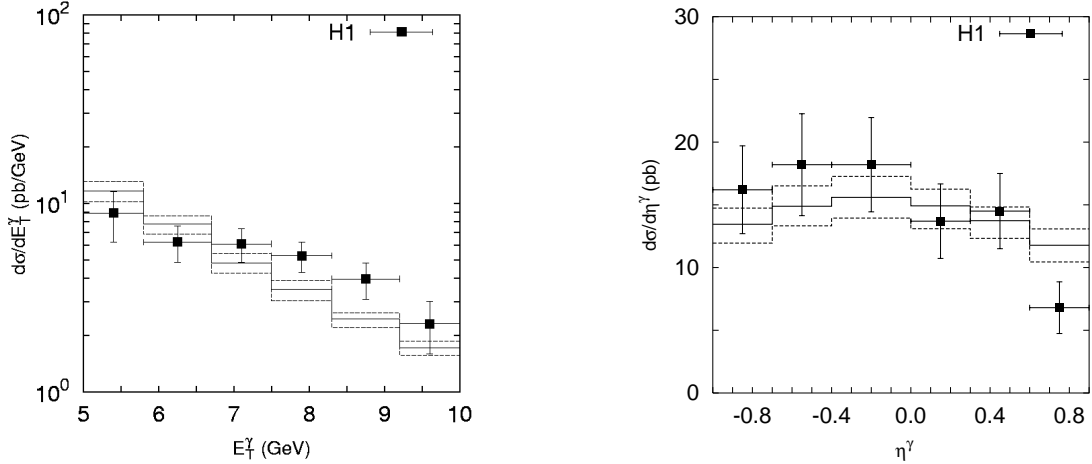


Fig. 8: Same as Fig. 7, but for γ +jet events with the additional jet cuts: $-1 < \eta^{\text{jet}} < 2.3$ and $E_T^{\text{jet}} > 4.5$ GeV.

The H1 experimental data in photoproduction [18] were also compared to the k_T -factorization approach [6]. Comparison with the k_T factorization approach indicates somewhat better agreement, as shown in Fig. 7 (see [6] for details). One can see that the measured distributions are reasonably well described except the moderate E_T^γ region and in the pseudorapidity region $-0.4 \leq \eta^\gamma \leq 0.9$ only. For $-1 \leq \eta^\gamma \leq -0.4$ the k_T -factorization predictions are mostly below the experimental points. The discrepancy between data and theory at negative η^γ is found to be relatively strong at low values of the initial photon fractional momentum y . The effect of scale variations in transverse energy distributions is rather large: the relative difference between results for $\mu = E_T^\gamma$ and results for $\mu = E_T^\gamma/2$ or $\mu = 2E_T^\gamma$ is about 15% within the k_T -factorization approach, which is due to missing higher order corrections. The scale dependence of the NLO QCD calculations in the collinear factorization approach is below the 10% level.

The individual contributions from the direct and resolved production mechanisms to the total cross section in the k_T -factorization approach is about 47% and 53%, respectively. The contributions of single resolved processes

$$\begin{aligned} q(k_1) + g(k_2) &\rightarrow \gamma(p_\gamma) + q(p'), \\ g(k_1) + q(k_2) &\rightarrow \gamma(p_\gamma) + q(p'), \\ q(k_1) + q(k_2) &\rightarrow \gamma(p_\gamma) + g(p'). \end{aligned}$$

account for 80%, 14% and 6% respectively.

The transverse energy E_T^γ and pseudorapidity η^γ distributions for γ +jet events measured by H1 are compared to the k_T -factorization predictions in Fig. 8 (see also Ref. [6]). In contrast to the inclusive case, one can see that the k_T -factorization predictions are consistent with the data in most bins, although some discrepancies are present. The theoretical results are lower than the experimental data at negative η^γ and higher at positive η^γ . The scale variation as it was described above changes the estimated cross sections by about 10%. Note that such disagreement between predicted and measured cross sections has also been observed for the NLO QCD calculations in the collinear factorization approach, see Fig. 6.

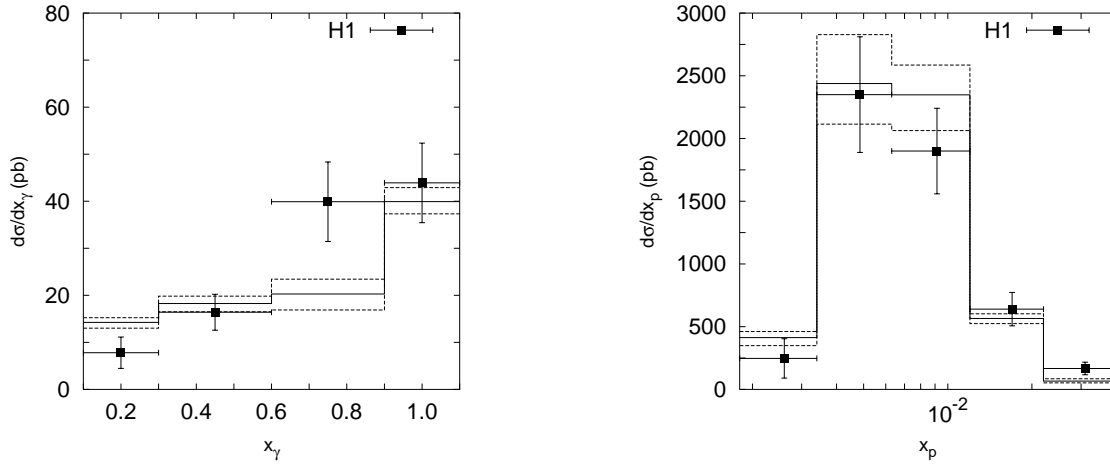


Fig. 9: The differential cross section $d\sigma/dx_\gamma$ and $d\sigma/dx_p$ of prompt photon + jet production calculated at $5 < E_T^\gamma < 10$ GeV and $0.2 < y < 0.7$ with an additional jet requirement $-1 < \eta^{\text{jet}} < 2.3$ and $E_T^{\text{jet}} > 4.5$ GeV.

Figure 9 shows the x_{obs}^γ and x_{obs}^p distributions (see Eq. 3) measured by H1. One can see that k_T factorization predictions reasonably well agree with the experimental data. The NLO calculations [3, 4] without corrections for hadronization and multiple interactions give similar results.

The H1 Collaboration [21] also has performed γ +jet measurements in DIS for $Q^2 > 4 \text{ GeV}^2$. The NLO calculations [22], which are only available for γ +jet final state, failed to describe normalization of the cross sections, although the agreement in shape was found to be reasonable (Fig. 10). No k_T factorization prediction available for DIS.

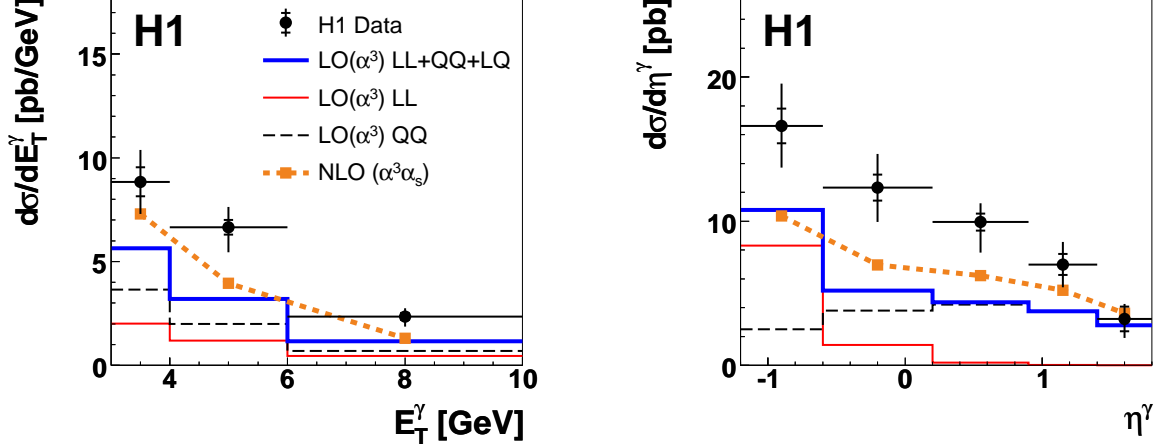


Fig. 10: The differential γ +jet cross sections as functions of E_T and η of the prompt photon in DIS. The data are compared to LO and NLO calculations.

In summary, some differences with NLO QCD were observed in both photoproduction and DIS. Differences at low P_T^γ can be due to the treatment of the fragmentation contribution in NLO calculations. Further, it would be interesting to see the effect of calculations beyond NLO QCD. The approach based on the k_T factorization has better agreement with the data, but such calculations have larger theoretical uncertainties.

5 Comparison with Tevatron results

Isolated photons in $p\bar{p}$ collisions at Tevatron have been measured recently by the CDF [23, 24] and D0 [25–28] Collaborations.

Measurements of $p\bar{p} \rightarrow \gamma + \text{jet} + X$ for $30 \text{ GeV} \leq p_T^\gamma \leq 300 \text{ GeV}$ have very recently been published by D0 [28]. The comparison to theory is done separately for different regions in rapidity of the photon and the jet. The NLO partonic Monte Carlo program JETPHOX [9, 29] was used to compare the data to theory at next-to-leading order. It was shown that the NLO calculations are not sufficient to describe the shape of P_T^γ distributions in different rapidity regions, as can be seen in Figure 11. At present, the comparison with the k_T -factorization prediction is in progress.

Differences with the collinear factorization approach have been seen previously as well. Both CDF [23] and D0 [26] cross sections were found to be above¹ NLO predictions at low P_T^γ . However, RHIC has also measured prompt photon production in pp collisions at $\sqrt{s} = 200 \text{ GeV}$ and found good agreement with NLO theory in the collinear factorization approach [20, 30].

The same data were compared to the k_T factorization approach in [13]. Figures 12 and 13 show the CDF [23] and D0 [26] measurements for the $d\sigma/dE_T^\gamma d\eta^\gamma$ cross sections calculated at $\sqrt{s} = 630$ and 1800 GeV in central and forward kinematic regions together with the k_T factorization predictions. One can see that theoretical predictions agree with the experimental data within the scale uncertainties. However,

¹For D0, the difference was mainly concentrated in the central rapidity region.

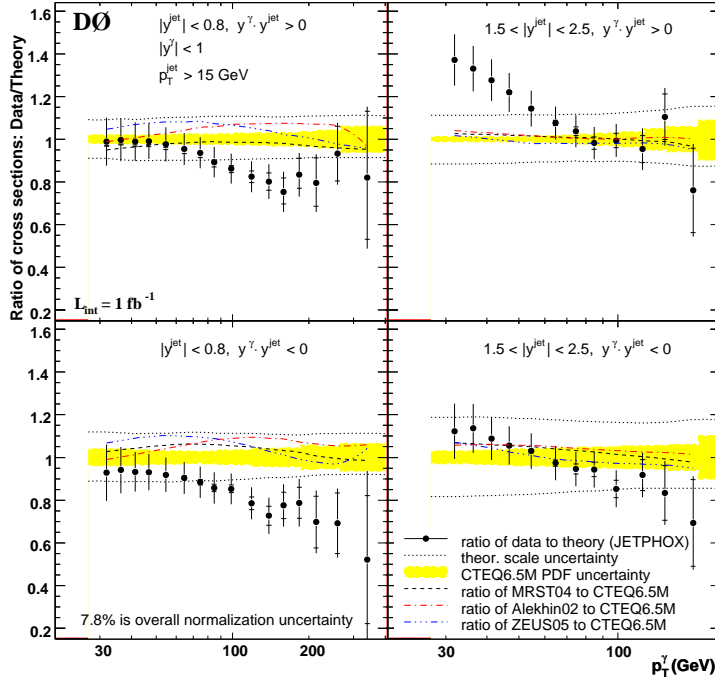


Fig. 11: The ratios of the triple-differential cross section measured by D0 compared to the NLO QCD prediction using JETPHOX. See details in Ref. [28].

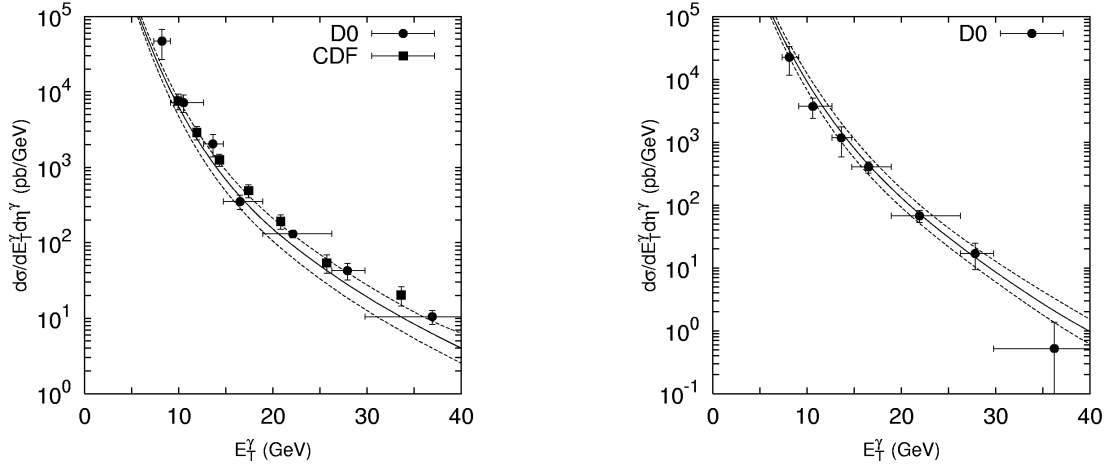


Fig. 12: The double differential cross section $d\sigma/dE_T^\gamma d\eta^\gamma$ of inclusive prompt photon production at $\sqrt{s} = 630$ GeV and $|\eta^\gamma| < 0.9$ (left plot) and $1.6 < |\eta^\gamma| < 2.5$ (right panel). The solid line corresponds to the default scale $\mu = E_T^\gamma$ of the k_T factorization predictions, whereas upper and lower dashed lines correspond to the $\mu = E_T^\gamma/2$ and $\mu = 2E_T^\gamma$.

the results of the calculation with the default scale tend to underestimate the data in the central kinematic region and agree with the D0 data in the forward η^γ region. The collinear NLO QCD calculations give a similar description of the data: generally there is a residual negative slope in the ratio of the data over the prediction as a function of E_T^γ . The scale dependence of the k_T factorization results is rather large (20 – 30%), due to the fact that these are leading order calculations.

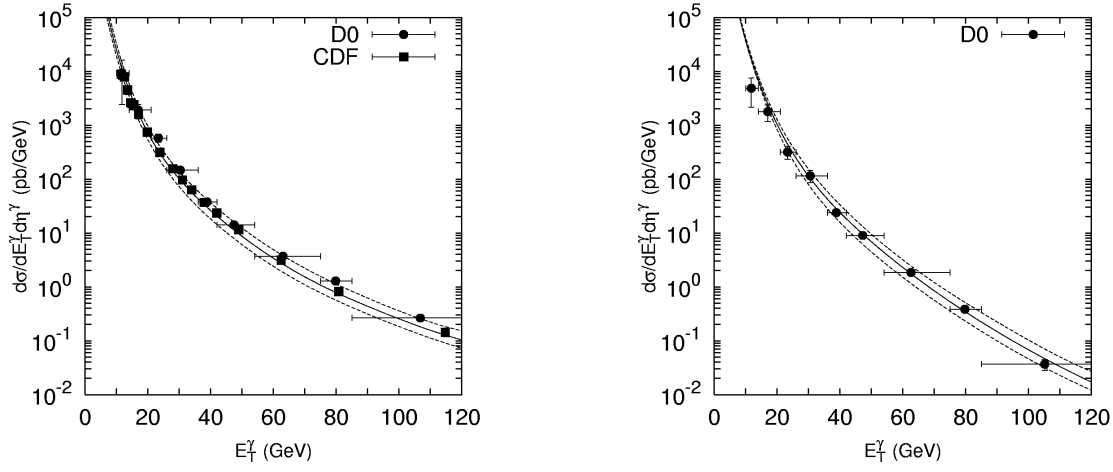


Fig. 13: The double differential cross section $d\sigma/dE_T^\gamma d\eta^\gamma$ of inclusive prompt photon production at $\sqrt{s} = 1800$ GeV and $|\eta^\gamma| < 0.9$ (left plot) and $1.6 < |\eta^\gamma| < 2.5$ (right plot). The solid line corresponds to the default scale $\mu = E_T^\gamma$, whereas upper and lower dashed lines correspond to the $\mu = E_T^\gamma/2$ and $\mu = 2E_T^\gamma$ for the k_T factorization calculations.

The double differential cross sections $d\sigma/dE_T^\gamma d\eta^\gamma$ are usually the most difficult observables to describe using QCD predictions. Yet, as it can be seen from Fig. 13, the k_T -factorization predictions agree well with D0 [25] and CDF [23] data both in shape and normalization. There are only rather small overestimations of the data at low E_T^γ values in Figs. 13 in the forward region. Again, the scale dependence of our calculations is about 20–30%. The theoretical uncertainties of the collinear NLO predictions are smaller (about 6% [25]), which is to be expected as inclusion of higher order terms reduces the scale uncertainty.

One can conclude that the results of calculations in the k_T -factorization approach in general agree well with Tevatron experimental data, within a large scale uncertainty.

6 Prompt photons at LHC

The direct photon production at LHC has significantly higher cross sections compared to the ones measured at Tevatron and HERA. The prompt-photon cross section at LHC is more than a factor of hundred higher than that at Tevatron and a factor of 10^5 larger than that for photoproduction at HERA, assuming a similar kinematic range ($|\eta^\gamma| < 2$), as shown in Fig. 14. This will allow to explore the TeV energy scale already in a few years of data taking.

Figure 15 shows the comparison between PYTHIA and HERWIG Monte Carlo models and JETPHOX LO and NLO calculations. The cross sections for $\gamma + jet$ events were calculated for $|\eta^\gamma| < 2$, $P_T^\gamma > 100$ GeV and $P_T^{jet} > 105$ GeV. The cuts on the transverse momenta are asymmetric to avoid instabilities in the NLO calculations. An isolation requirement $E_T^\gamma > 0.9 E_T^{tot}$ was imposed, where E_T^{tot} is the total energy of the jet which contains prompt photon. Jets were reconstructed with the longitudinally-invariant k_T algorithm in inclusive

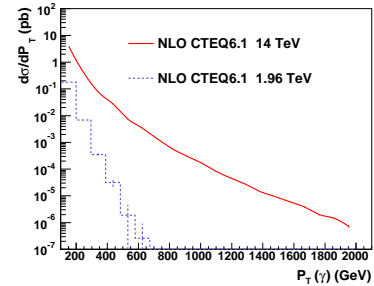


Fig. 14: The P_T^γ cross section for $\gamma+jet$ events predicted by NLO QCD for the Tevatron and the LHC kinematic range.

mode [31].

The NLO QCD calculation is 30–40% higher than that predicted by PYTHIA. On the other hand, PYTHIA is 20% above HERWIG. It is interesting to observe that the level of discrepancy between PYTHIA and HERWIG is about the same as that observed at HERA at much lower transverse momenta (for example see Fig. 4). However, there is no significant difference between NLO and PYTHIA at $P_T^\gamma > 10$ GeV for ep , while at the LHC energy range the difference between NLO and PYTHIA is rather significant. Certainly, the overall normalization of Monte Carlo programs like PYTHIA or HERWIG has to be adjusted, as these programs cannot account for contributions from loop corrections at higher orders.

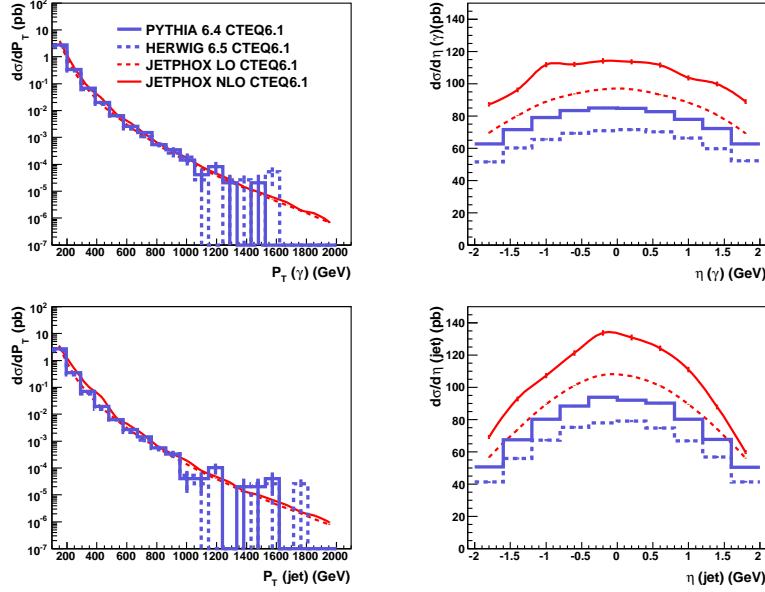


Fig. 15: Comparisons of Monte Carlo models with LO and NLO calculations as implemented in JETPHOX.

Scale uncertainties were estimated by changing the renormalization and factorization scales in the range $0.5 < \mu_f, \mu_R < 2$. The relative difference between predicted cross sections is shown in Fig. 16. To make quantitative statements on scale uncertainties with the present level of statistical errors in calculations using JETPHOX, a linear fit was performed to determine the trend of the relative differences with increase of P_T^γ . As it can be seen, the scale uncertainty is about 10% and slowly increases with P_T^γ .

To estimate the uncertainty associated with the gluon density, the calculations have been performed using two CTEQ6.1M sets (15 and 30) which correspond to two extremes in the gluon density at large x [32]. Fig. 17 shows the relative difference between those two sets as a function of P_T^γ . It is seen that the gluon uncertainty is almost a factor of two larger compared to the scale uncertainty estimated above. No statistically significant difference has been observed between the cross sections calculated using CTEQ6.1M and MRST04. This is not totally surprising as both sets have similar input data for the global fit analysis.

The predictions for the k_T factorization approach were obtained for a wider pseudorapidity range, for both central and forward pseudo-rapidities η^γ . As a representative example, we will define the central and forward kinematic regions by the requirements $|\eta^\gamma| < 2.5$ and $2.5 < |\eta^\gamma| < 4$, respectively. The transverse energy E_T^γ distributions of the inclusive prompt photon production in different η^γ ranges at $\sqrt{s} = 14$ TeV are shown in Figs. 18. One can see that variation in scale μ changes the estimated cross

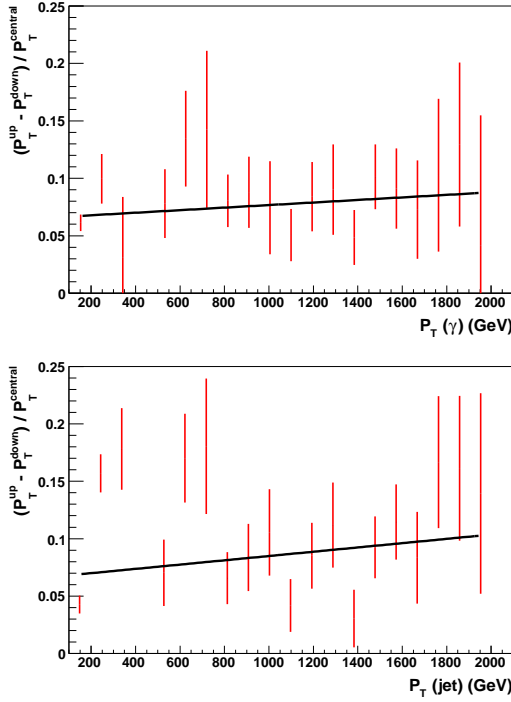


Fig. 16: Relative difference between the cross section estimated with $\mu = 0.5$ (P_T^{up}) and $\mu = 2$ (P_T^{down}) as a function of P_T for gamma and jet. The line represents a linear fit.

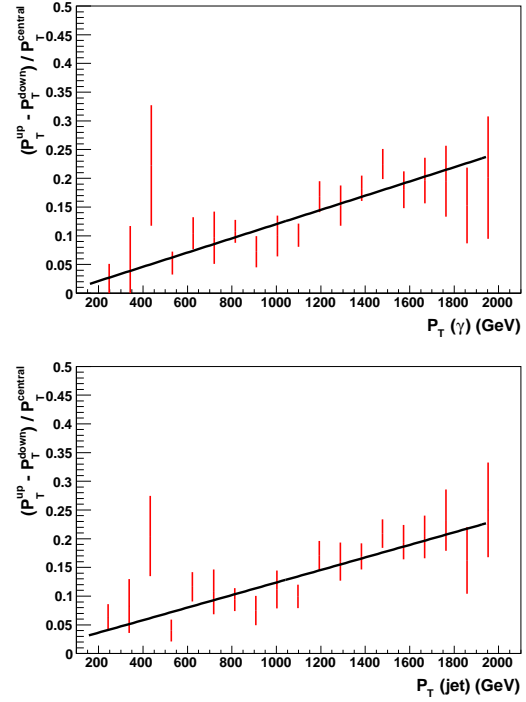


Fig. 17: Relative difference between the cross section estimated with CTEQ6.1M set=15 (P_T^{up}) and set=15 (P_T^{down}) as a function of P_T for gamma and jet. The line represents a linear fit.

sections by about 20–30%. However, as it was already discussed above, there are additional theoretical uncertainties due to the non-collinear parton evolution, and these uncertainties are not well studied up to this time. Also the extrapolation of the available parton distribution to the region of lower x is a special problem at the LHC energies. In particular, one of the problem is connected with the correct treatment of saturation effects in small x region. Therefore, more work needs to be done until these uncertainties will be reduced.

Thus, the calculation based on the k_T factorization approach shows a larger scale uncertainty compared to the collinear factorization approach: for $P_T^\gamma \sim 100$ GeV, the overall uncertainty for the NLO calculations is expected to be around 10%, while it reaches 20–30% for the k_T -factorization calculations for the same P_T^γ range, due to the fact that the latter are at leading order in α_s . As the residual scale dependence of missing higher order terms resides in logarithms involving ratios of P_T^2 and scales μ^2 , the effect becomes more dramatic at the LHC energy.

7 Summary

In this review, we have attempted to summarize recent progress in the description of prompt photon production at HERA, the Tevatron and the LHC. At HERA, some differences with NLO were observed in both photoproduction and DIS. The deficiencies at low P_T^γ values may indicate that non-perturbative effects at small P_T^γ play a non-negligible role. Also, one should expect that adding high-order corrections to the collinear-factorization approach should improve the description. Similar conclusions can be drawn for the Tevatron data which, as in the HERA case, has differences with NLO in the lowest P_T^γ region. Recently, significant differences with NLO were observed by the Tevatron for the shapes of P_T^γ

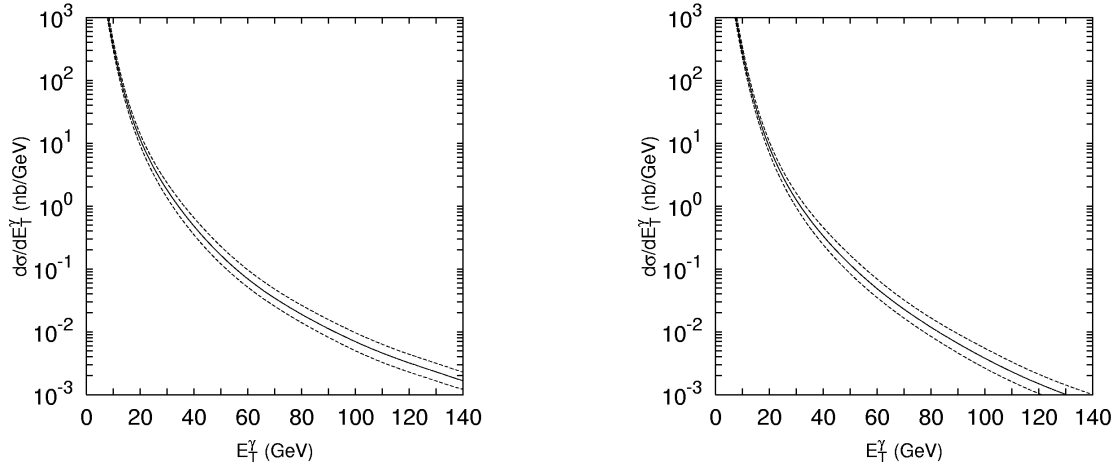


Fig. 18: Left plot: The k_T factorization predictions for differential cross sections $d\sigma/dE_T^\gamma d\eta^\gamma$ at $\sqrt{s} = 14$ TeV GeV and $|\eta^\gamma| < 2.5$ (left plot); at $2.5 < \eta^\gamma < 4.0$ (right plot). The solid line corresponds to the default scale $\mu = E_T^\gamma$, whereas upper and lower dashed lines correspond to the $\mu = E_T^\gamma/2$ and $\mu = 2E_T^\gamma$.

distributions differential in η^γ . On the other hand, RHIC observes good agreement with NLO QCD. Considering the fact that RHIC uses a photon isolation method which is different from the usual cone isolation, the differences mentioned above may also have to do with isolation criteria acting differently in a partonic calculation than in the full hadronic environment of the experiment.

An alternative approach based on the k_T factorization generally improves the description of the HERA and the Tevatron data, but it has larger theoretical uncertainties. As for NLO, high-order corrections to the k_T -factorization approach should improve the description of the data. The applicability of the k_T factorization to the LHC data will be tested with the arrival of the first LHC data, but it is already evident that significant theoretical uncertainties are expected for the description of prompt-photon cross sections at LHC. Using the collinear factorization approach, uncertainties of NLO calculations are expected to be 10–20% at about 1 TeV photon transverse momenta, and significantly larger for the k_T -factorization calculations. These uncertainties have to be reduced in the future for detailed comparison of the LHC data with the QCD predictions.

In all cases, Monte Carlo predictions fail to describe prompt-photon cross sections, both in shape and normalization. Generally, HERWIG is significantly below PYTHIA. This could have a direct impact on the future LHC measurements, in particular for exotic searches which often rely on Monte Carlo predictions for estimations of rates for background events.

This work supported in part by the U.S. Department of Energy, Division of High Energy Physics, under Contract DE-AC02-06CH11357.

References

- [1] J. F. Owens, Rev. Mod. Phys. **59**, 465 (1987).
- [2] L. Gordon and W. Vogelsang, Phys. Rep. **D52**, 58 (1995).
- [3] M. Krawczyk and A. Zembrzusi, Phys. Rev. **D64**, 14017 (2001).
- [4] M. Fontannaz, J. P. Guillet, and G. Heinrich, Eur. Phys. J. **C21**, 303 (2001).
- [5] M. Fontannaz and G. Heinrich, Eur. Phys. J. **C 34**, 191 (2004).
- [6] A. Lipatov and N. Zotov, Phys. Rev. **D72**, 054002 (2005).
- [7] C. F. von Weizsacker, Z. Phys. **88**, 612 (1934).
E. J. Williams, Phys. Rev. **45**, 729 (1934).
- [8] M. Fontannaz, J. P. Guillet, and G. Heinrich, Eur. Phys. J. **C 22**, 303 (2001).
- [9] PHOX programs. Available at http://lappweb.in2p3.fr/lapth/phox_family/main.html.
- [10] A. Zembrzusi and M. Krawczyk, Photoproduction of isolated photon and jet at the DESY HERA, 2003, hep-ph/0309308.
- [11] ZEUS Collaboration, S. Chekanov *et al.*, Phys. Lett. **B511**, 19 (2001).
- [12] E. M. Levin *et al.*, Sov. J. Nucl. Phys. **53**, 657 (1991).
S. Catani, M. Ciafaloni, and F. Hautmann, Nucl. Phys. **B366**, 135 (1991).
J. Collins and R. Ellis, Nucl. Phys. **B360**, 3 (1991).
- [13] A. V. Lipatov and N. P. Zotov, J. Phys. **G34**, 219 (2007).
- [14] M. A. Kimber, A. D. Martin, and M. G. Ryskin, Phys. Rev. **D63**, 114027 (2001).
G. Watt, A. D. Martin, and M. G. Ryskin, Eur. Phys. J. **C31**, 73 (2003).
- [15] ZEUS Collaboration, S. Chekanov *et al.*, Eur. Phys. J. **C49**, 511 (2007).
- [16] T. Sjostrand, S. Mrenna, and P. Skands, JHEP **05**, 026 (2006).
- [17] G. Corcella *et al.*, JHEP **01**, 010 (2001).
G. Corcella *et al.*, (2002), hep-ph/0210213.
- [18] H1 Collaboration, A. Aktas *et al.*, Eur. Phys. J. **C38**, 437 (2005).
- [19] ZEUS Collaboration, J. Breitweg *et al.*, Phys. Lett. **B472**, 175 (2000).
- [20] G. Heinrich, Proceedings of the International Conference Photon2007, Paris, France (2007).
- [21] H1 Collaboration, F. D. Aaron *et al.*, Eur. Phys. J. **C54**, 371 (2008).
- [22] A. Gehrmann-De Ridder, G. Kramer, and H. Spiesberger, Nucl. Phys. **B578**, 326 (2000).
- [23] CDF Collaboration, D. E. Acosta *et al.*, Phys. Rev. **D65**, 112003 (2002).

- [24] CDF Collaboration, D. E. Acosta *et al.*, Phys. Rev. **D70**, 074008 (2004).
- [25] D0 Collaboration, B. Abbott *et al.*, Phys. Rev. Lett. **84**, 2786 (2000).
- [26] D0 Collaboration, V. M. Abazov *et al.*, Phys. Rev. Lett. **87**, 251805 (2001).
- [27] D0 Collaboration, V. M. Abazov *et al.*, Phys. Lett. **B639**, 151 (2006).
- [28] D0 Collaboration, V. M. Abazov *et al.*, (2008), hep-ex/0804.1107.
- [29] P. Aurenche, M. Fontannaz, J.-P. Guillet, E. Pilon, and M. Werlen, Phys. Rev. **D73**, 094007 (2006).
- [30] PHENIX Collaboration, S. S. Adler *et al.*, Phys. Rev. Lett. **98**, 012002 (2007).
- [31] S. Ellis and D. Soper, Phys. Rev. **D48**, 3160 (1993).
S. Catani *et al.*, Nucl. Phys. **B406**, 187 (1993).
- [32] D. Stump *et al.*, JHEP **310**, 46 (2003).